Simulating the MilliQan Detector via Geant4

R. Schmitz

October 17, 2019

1 Introduction

In this document, I briefly describe the motivations and techniques for full detector simulation using Geant4 as it applies to the MilliQan experiment. I'll outline the general structure of the simulation, describing its basic purpose and how it functions. I'll also source the various spectra and properties implemented in the simulation at various stages. Finally, I'll discuss the intended subjects of study and how this simulation approaches them.

2 Geant4 MilliQan Simulation Feature Overview

The goal of the Geant4 detector simulation is to take a pre-defined set of fractionally charged particle tracks collected by the "propagation effort" (whether via Pythia, some Python script, etc.) and explicitly propagate those through the detector, shown in Figure 1. It can do this by defining a custom particle which is endowed with a specified amount of charge, then propagating that particle through the detector and tracking the scintillation photons which result from its interactions [NOTE: This feature is yet to be implemented. Still need to port it from the previous Geant simulation that was in use]. The chief interest of the simulation, then, is in appropriately propagating scintillation photons through the detector, and ensuring that the PMT detection efficiency is properly modeled. *We currently explicitly track neutrons, muons, electrons, mCPs, optical photons, and gammas through the simulation, and we implement the Geant4 ShieldingPhysicsList as our simulation physics list.*

In order to simulate generation and propagation of scintillation photons correctly, we must focus on the validation of a single bar. In particular, we need to (1) generate the proper number of scintillation photons as a charged particle passes through a bar, and (2) propagate those photons appropriately to the detector. The first problem is handled by the scintillation yield and scintillation spectrum of the material. This scintillation yield is described by two parameters: the absolute scintillation yield of the material (total number of photons), and the scintillation spectrum of the material (distribution of photon wavelengths). We are studying EJ-200 scintillator, a general purpose scintillator with "a long attenuation length and a scintillation spectrum well-matched to common PMTs" [1]. The key properties of this scintillator are a scintillation yield of 10000 photons per 1 MeV electron, 3.8m bulk light attenuation length, 1.58 refractive index, and a scintillation spectrum given in Figure 2.

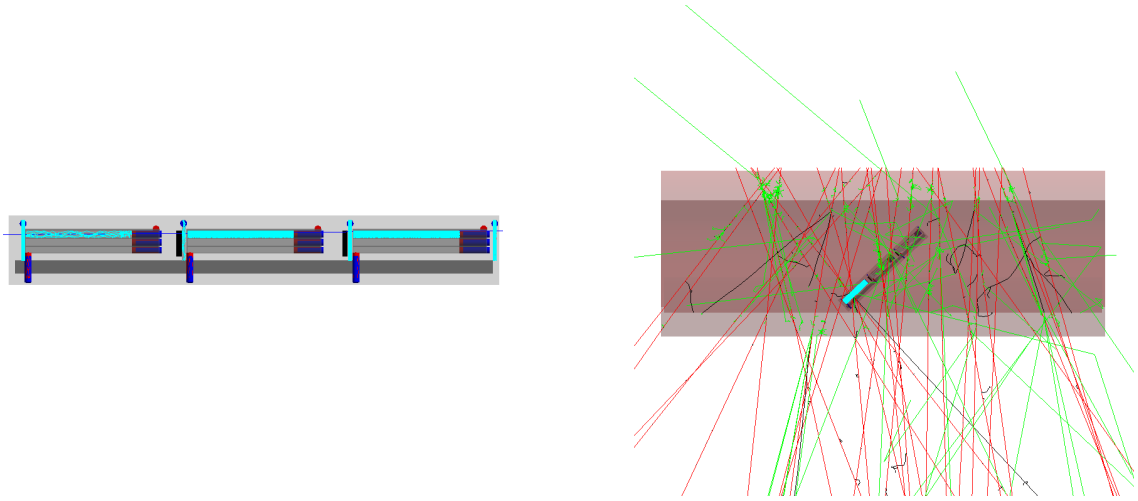

(a) MilliQan detector with a throughgoing mCP

(b) Muon showers in the cavern

Figure 1: The full MilliQan detector consists of an array of single scintillator bars. We study the light collection properties of the individual bars in order to evaluate the overall millicharged particle detection efficiency of the (a) full detector, and in particular study the response of the detector (b) inside the cavern, as incident muons interact with the cavern walls to produce showers.

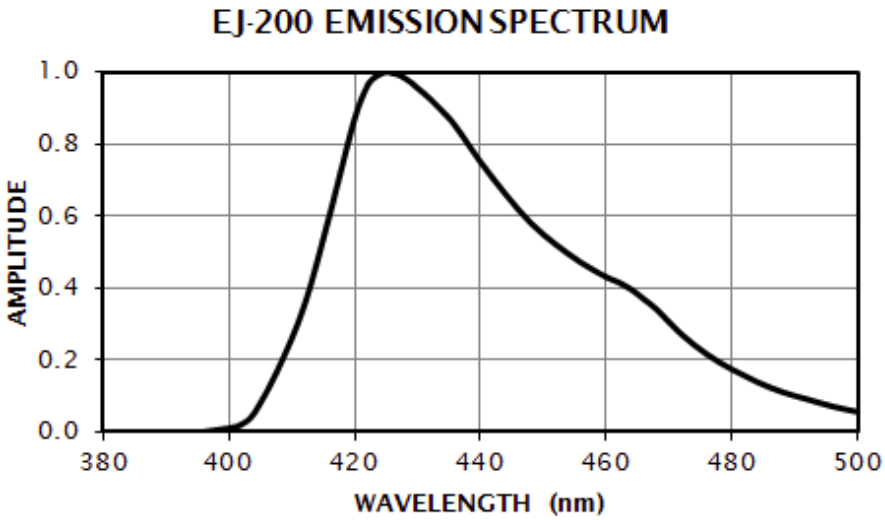

Figure 2: Scintillation spectrum from EJ-200 Scintillator. The spectrum peaks at 425 nm.

After we have properly generated the right number of photons, we need to ensure that we detect the right number of photons. In particular, we want the photon detection number to be correct even as a function of initial scintillation photon position. To do this, we must propagate the correct number of photons to the detector, and then we must detect the appropriate fraction of incoming photons.

To propagate photons appropriately, we need to account for each source of photon ab-

sorption in the scintillator bar. There are two major considerations here: absorption in the bulk of the scintillator, and absorption in the scintillator wrapping material. The former is handled by simply implementing the 3.8m bulk light attenuation length of the material. The latter is a bit more tricky.

First, we add in an air gap layer between the wrapping material and the scintillator, as without a specific material gluing the wrapping to the scintillator we are likely to see an airgap be formed. We study two different types of wrapping materials: Tyvek paper and Teflon wrapping. Tyvek tends to form a larger airgap during the wrapping procedure since it is more rigid than Teflon, so its airgap is 1mm as opposed to 0.2 mm for Teflon. These air gap sizes are approximate, but being exact in the sizing is not particularly important since the most impactful feature of an airgap is the creation of a scintillator-air interface which facilitates total internal reflections. By specifying the index of refraction of the scintillator as 1.58 in accordance to its datasheet value, we appropriately account for this scintillator-air interface.

Second, we use the UNIFIED model Geant4 reflection model to account for reflections across the air-wrapping interface. This model contains both air-to-Tyvek and air-to-teflon reflectivity spectra. Each of these spectra can be further refined to "polished" (closer to specular) or "ground" (closer to diffuse) spectra, depending on the material interface. I choose ground-type reflections for the wrapping material because white pieces of Tyvek and Teflon seem to reflect photons uniformly, but changes to the polished vs. ground reflectivity scheme do not make a detectable difference in the final photon detection counts so this choice is somewhat arbitrary. One characteristic of note of Tyvek and Teflon that is accounted for using this approach is their angular dependence on diffuse vs. specular reflections. That is, for sharper angles of incidence light is more likely to be reflected specularly (i.e. geometry preserving) rather than diffusely (isotropic). These details are discussed in [2]. Additionally, the reflectivity for Tyvek and Teflon is approximately constant in the optical range, and is given by $R_{Tyvek} = 0.97$ and $R_{Teflon} = 0.99$ [3].

Finally, we must properly detect photons which arrive at the PMT from the scintillator. First, as we are using a Hamamatsu R878 PMT, we take the quantum efficiency of the PMT from measurements done on the R878, shown in Figure 3 [4]. PMT tubes of model R7725 by Hamamatsu and ET9418B by ET Enterprises are also used in the MilliQan demonstrator, so we include their spectra in the simulation as well.

When a photon encounters the PMT, the simulation kills the photon track and applies the (wavelength-dependent) quantum efficiency to it. Whether it is successfully detected or not, the photon track is removed the moment this quantum efficiency is applied. Also, in order to encounter the PMT, the photon must pass through the scintillator-PMT interface and interact with the photocathode. Photons which are incident on the PMT from large angles are likely to be rejected, as the detection efficiency of Hamamatsu PMTs are highly angle dependent as shown in Figure 4 [5].

If a photon passes through both of these detection efficiencies, it is detected. To verify the veracity of the simulation, we compare its performance for simulated muons of energy 4 GeV on a single bar to muon telescope data collected under the same geometric parameters on an experimental equivalent scintillator bar. By adjusting the exact reflectivity and scintillation yield of our scintillator and by measuring the results for two bars, we can establish the expected variance for scintillation yield and light collection efficiency in the MilliQan bars.

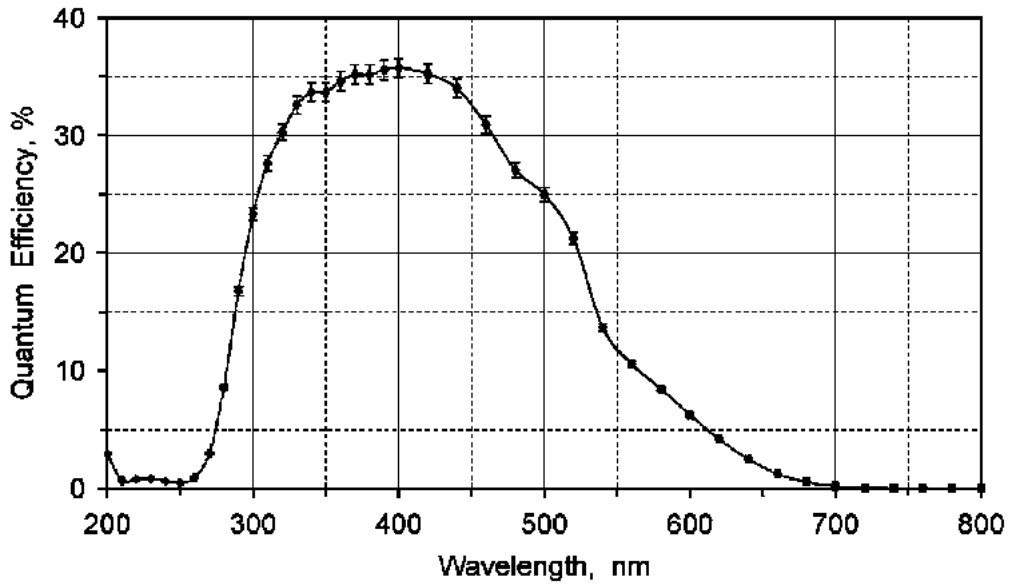

Figure 3: Quantum Efficiency of Hamamatsu R878 PMT.

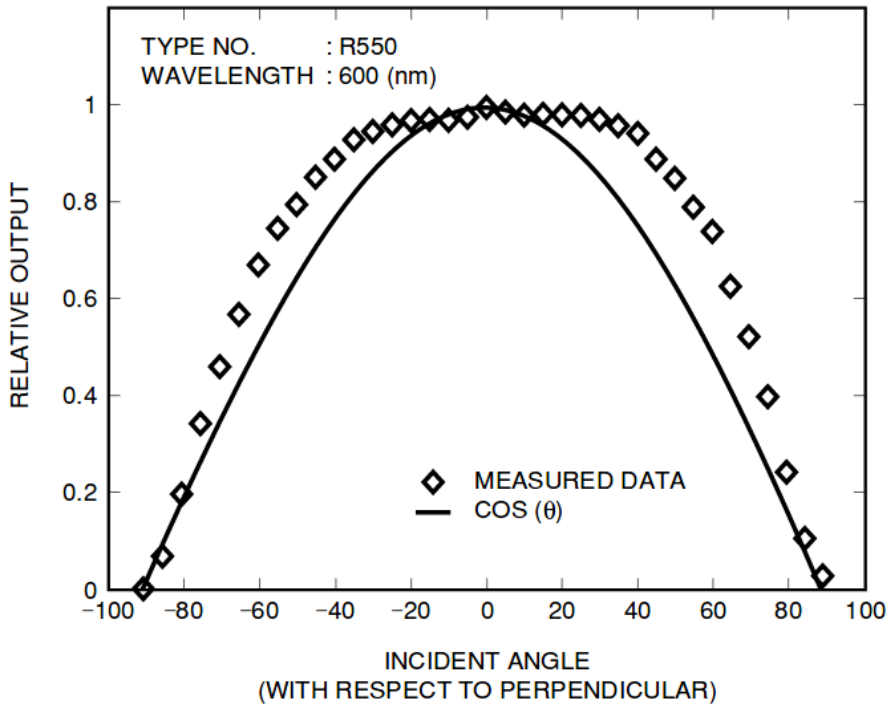

Figure 4: Angular Detection Efficiency of Hamamatsu PMTs. In order to interact with the photocathode, the photon must pass through this angular detection efficiency first. Note that the angular detection efficiency is approximately described by a $\cos(\theta)$ distribution. The information here is derived from a writeup published by Hamamatsu [5].

It also allows us to identify the parameters which maximize realism when comparing Geant to experimental data.

In addition to simulating the MilliQan bars, it is useful to simulate all other features of the MilliQan detector. The MilliQan demonstrator detector that is currently installed at CERN has several optically relevant features, as shown in Figure 5.

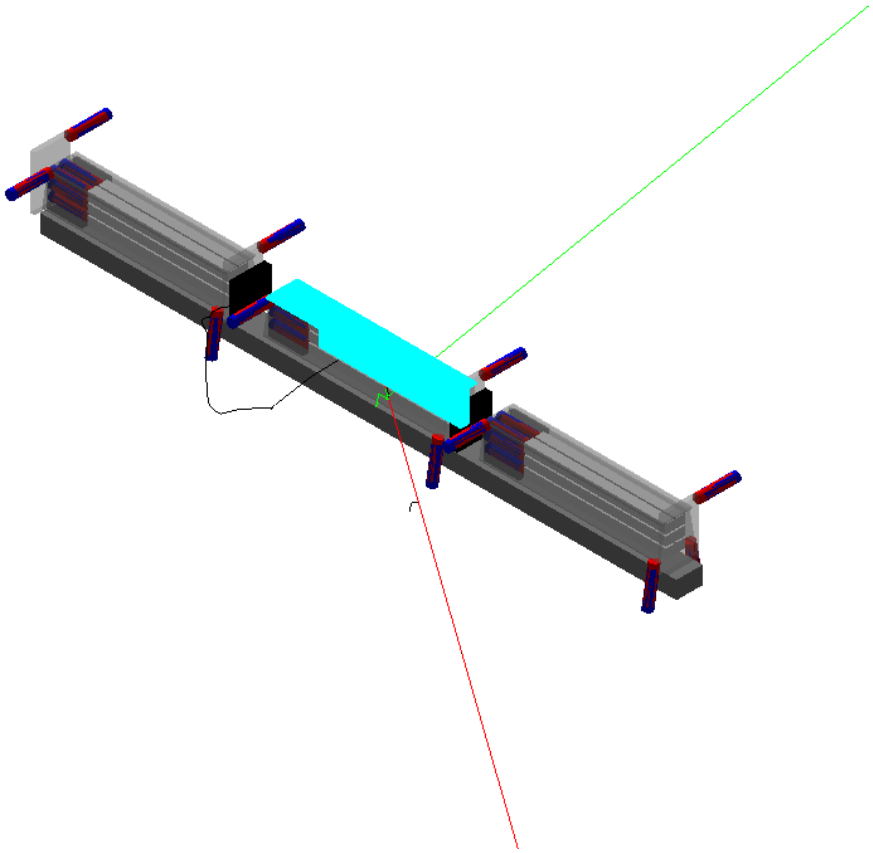

Figure 5: A Geant4 model of the MilliQan Demonstrator.

Notable detector geometry features included in the Geant4 simulation include lead and scintillator slabs in between each of the detector layers, as well as scintillator panels located above, to the left, and to the right of each of the layers. A hodoscope is located on the far ends of the detector to provide a tracking comparison to experiment. Wrapping each PMT stack is a layer of mu-metal, used as magnetic shielding. Finally, each scintillator shielding layer is complete with PMT readout placed in the same location as in the demonstrator. Treating these scintillator slabs in the same way as we treat the bars, we can examine the veto performance of the detector to various backgrounds.

We also simulate the surrounding environment of the detector. The cavern around the detector is made of concrete. The cavern is modeled as a 3.6m inner-radius cylinder with a 2m tall by 3.2m wide rectangular cutout centered on the bottom of the cylinder running

along its length (i.e. the cutout is centered 1.8m below the axis of the cylinder). This shape forms a cavern with cylindrical walls/ceiling and a flat, rectangular floor as shown in Figure 6. Finally, there is also accompanying magnetic field in the cavern which is given by $B(x, y, z) = (-1.61, -1.73, 21.57)$*Gauss, where +x points vertically upwards, +z points to the right with respect to Figure 1b, and +y points into the page with respect to Figure 1b. Note that the detector itself is tilted 43.1 degrees above the horizontal (z-axis) in order to point directly towards the CMS interaction point in the physical experiment.

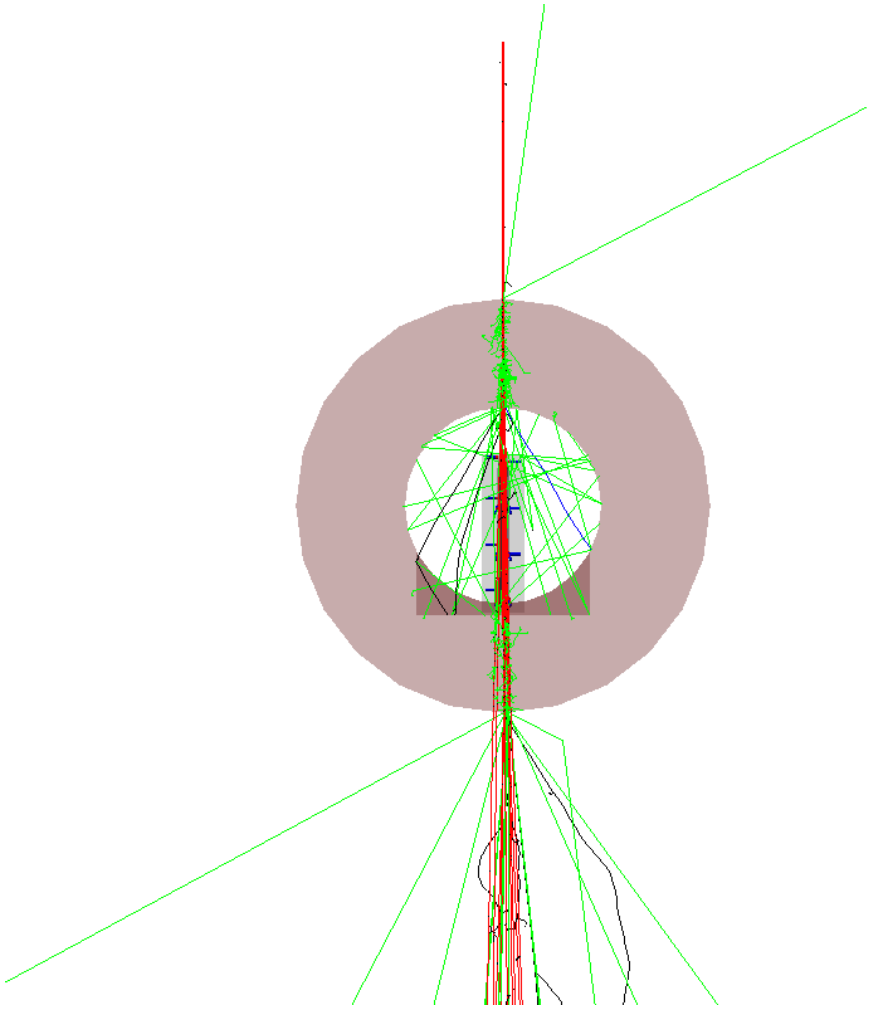

Figure 6: A side view of the detector in the MilliQan cavern.

Additionally, an array of datastructures are produced by the simulation. There are three fundamental types of accessible datastructures: Hit-level data, which are populated by a single entry per sensitive detector interaction; Track-level data, which are populated with a single entry per particle track; and Event-level data, which are populated with a single entry per event.

Hit-level data accessible to the simulation currently includes full timing and particle information for two types of hits: PMT Hits, where a photon is detected successfully by a PMT, and Scint Hits, which populate when a muon or mCP passes through a scintillator.

In each case, timing and geometric information is saved (i.e. when it happened and in which bar). For the case of the PMT hit, we save the photon's history so we can trace back the process which generated it. For the Scint hit, we save energy deposition in the scintillator layers, as well as the exact track length a muon or mCP took as it passed through a bar, slab, or panel of scintillator.

Track-level data accessible to the simulation includes particle energies, initial positions, generating processes, and interaction information. For electrons, for example, we know where they were generated, which particle generated them, which daughters the electron produced, and how much overall energy it deposited in a particular layer. Similar information is available to other types of particle tracks. Photon tracking information is also available, though it dramatically increases the size of the output files.

Event-level information are the most useful parameters generated by the simulation. This includes how many PMT Hits happened in different volumes, how many electrons/photons/gammas were generated by the incident muon, trigger information about whether or not an experimental equivalent of the event would register a trigger, and a lot more.

3 MilliQan Simulation Studies

Using all the geometric information together with the output datastructures, we study three different incident particle sources using this simulation: cosmogenic muons, collision muons, and collision mCPs. In this context, "collision" means "generated by the nearby CMS interaction point". The first two studies look at muons, how their shower products interact with the detector, and in particular whether or not muon showers may resemble mCP signals. The mCP study itself looks at the expected signal produced in the detector by a throughgoing collision mCP for an array of different mCP charges and masses, which allows for an improved background veto design as well as a more efficient, targeted handle on rejecting background for different mCP characteristics in experimental data analysis.

To study cosmogenic muons, a general distribution of angles and energies for incident muons are required. One such distribution for muons at the surface of the Earth is given by Gaisser, shown in Figure 7 [6]. Since the detector is located 40m underground and since muons lose 0.5 GeV per meter of energy, the energy distributions of muons which make it through to the detector goes as $E = 20sec(\theta)$. This means that $Ecos(\theta)$ is constant, so the distribution as a function of solid angle goes like $cos^{2.7}(\theta)$. Accounting for the solid angle correction divides out a $cos(\theta)$ term, yielding a distribution in angles that goes like $cos^{1.7}(\theta) \approx cos^{2}(\theta)$. A simulation using this distribution is shown above in Figure 1b. Note that the presence of the cavern is relevant here, as the showers produced by the incident muons emerge from the cavern walls.

$$\frac{dN_\mu}{dEd\Omega} \approx 1400 E_\mu^{-2.7} / (\mathrm{m^2 sGeV sr}) \left(\frac{1}{1 + \frac{1.1\mathrm{E}\cos\theta}{\epsilon_\pi}} + \frac{0.054}{1 + \frac{1.1\mathrm{E}\cos\theta}{\epsilon_\mathrm{K}}} \right)$$

Figure 7: Gausser approximation for muon energies and angular distributions.

To study collision muons, we require trajectories propagated from the CMS interaction point to the detector itself. This is done by the "propagation effort" alluded to above, mostly by Bennett Marsh. These trajectories specify the momentum fourvectors for the incident muons, including energy and 3-momentum as well as initial x,y,z location at which the muon is generated. The trajectories are also accompanied by associated generating processes: via W production, Drell-Yan (DY), QCD, or non-BC QCD. Each of these processes has an associated weight, so we can meaningfully determine the rate at which different muon events interact in different ways in the detector. The exact generation point for these muons is a 0.5m by 0.5m plane located 2m away from the detector face; most of these muons still have to pass through rock to make it to the detector, so this point is chosen to allow the muons to accumulate these shower products first. Other studies on collision muons may look at pencil beams of muons generated at other locations (e.g. 1m below, above, or to the side of the axis of the detector), but the idea is the same: read in trajectories in some plane, propagate them through rock, and look at the shower products at the detector. A sample beam muon trajectory is shown in Figure 8.

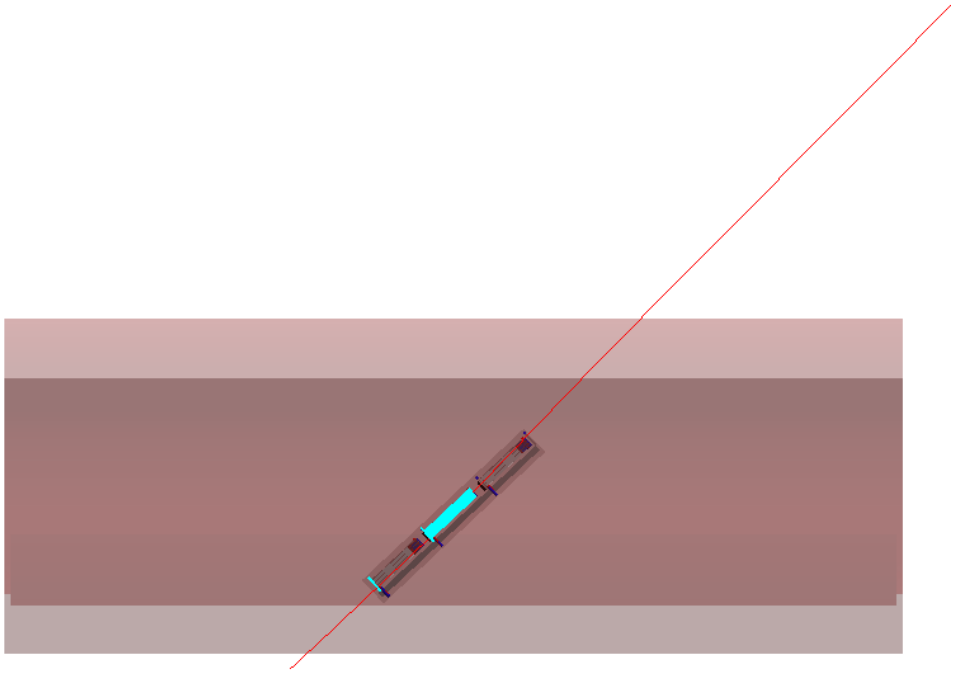

Figure 8: Gausser approximation for muon energies and angular distributions.

Finally, to study mCPs, a similar approach as for the collision muons is employed: mCP

trajectories are propagated from the CMS interaction point until they reach the detector. Once again, event weights are assigned for each generating process (rho, DY, jpsi, etc.), though many more processes are accounted for during mCP generation. Additionally, an entire grid of mCP charge and mass points are studied: masses from 0.01 GeV up to 10 GeV, and charges from 0.005 to 0.3, where the charge is cited as a fraction of the electron charge. One such example of an mCP incident on the MilliQan detector (zoomed in and rotated) is shown in Figure 1a. Here, the presence of the cavern walls is not as important since the mCPs interact with the walls only very rarely. Looking at PE production in the bars, slabs, and panels allows us to establish differnt trigger approaches. For example, should we require that no PE are detected in slabs to reject muons/electrons, or should we require that at least one nPE is registered in a slab to reject electronic background? These questions are complex and have different answers for different mCP charge/mass parameters, but this type of information allows for searches that can be tailed towards each section of the charge/mass mCP phase space.

In summary, the Geant4 simulation of the MilliQan detector manages every aspect of detector simulation and photon propagation, from the shower products produced by cavern walls to angular detection efficiency corrections for photons incident on PMTs. By interfacing with the propagation effort to retrieve muon and mCP trajectories, the simulation can accurately recreate expected responses in the detector for both mCP signals and muon backgrounds. Finally, these outputs can be interfaced with the analysis and experimental design efforts to improve the detection efficiency and expand the accessible regions of mCP charge/mass phase space. Iteration between simulation, design, and analysis allows for the best possible construction of the MilliQan experiment.

References

[1] Eljen Technology, "GENERAL PURPOSE EJ-200, EJ-204, EJ-208, EJ-212", EJ-200 datasheet, Accessed July 2019.

[2] M. Janecek and W. W. Moses, Optical reflectance measurements for commonly used reflectors, IEEE Trans. Nucl. Sci. , vol. 55, no. 4, pt. 2, pp. 24322437, Aug. 2008

[3] M. Janecek, W. W. Moses, Simulating Scintillator Light Collection Using Measured Optical Reflectance, IEEE T. Nucl. Sci. 57 (3), 964-970 (2010).

[4] Mirzoyan, Razmik Laatiaoui, Mustapha Teshima, M. (2006). Very high quantum efficiency PMTs with bialkali photo-cathode. Nuclear Instruments and Methods in Physics Research Section A: Accelerators, Spectrometers, Detectors and Associated Equipment. 567. 230232. 10.1016/j.nima.2006.05.094.

[5] Hamamatsu Photonics. "Photomultiplier Tubes: Basics and Applications". Third Edition (3a). p.62. 2007.

[6] Shukla and Sankrith. "Energy and angular distributions of atmospheric muons at the Earth." arXiv:1606.06907v3. 27 Sep 2018.